N88-23229

PIEZOELECTRIC PUSHERS FOR ACTIVE VIBRATION CONTROL OF ROTATING MACHINERY

Alan B. Palazzolo* and Albert F. Kascak
U.S. Army Aviation Research and Technology Activity - AVSCOM
Structural Dynamics Branch
NASA Lewis Research Center

ABSTRACT

The active control of rotordynamic vibrations and stability by magnetic bearings and electromagnetic shakers has been discussed extensively in the literature. These devices, though effective, are usually large in volume and add significant weight to the stator. The use of piezoelectric pushers may provide similar degrees of effectiveness in light, compact packages.

Tests are currently being conducted at the NASA Lewis Research Center with piezoelectric pusher-based active vibration control. The paper presents results from tests performed on the NASA test rig as preliminary verification of the related theory.

*Texas A&M University, College Station, Texas.

MODEL OF PIEZOELECTRIC PUSHER

A piezoelectric pusher consists of a stack of piezoelectric ceramic disks that expands in response to an applied voltage. The extension and force of the pusher depends on the number and thickness of the disks and on the cross sectional area of the disks, respectively.

The ideal model consists of a prescribed displacement α, which is proportional to the input voltage, and a spring representing the stiffness of the stack.

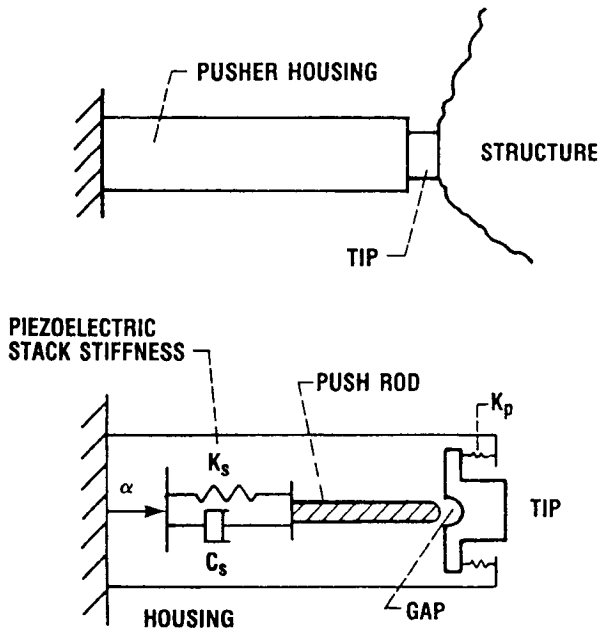

CD-88-32859

DEFLECTION VERSUS INPUT VOLTAGE

The figure shows a typical voltage versus tip displacement plot for the pusher in the previous figure. The curve in this plot provides an approximate description of the internal displacement α versus voltage relation, since the tip is unloaded and since the preload spring in the previous figure is very light (114 lb/in.). Therefore, it is assumed that the voltage sensitivity for α is $S_A = -1448$ V/in.

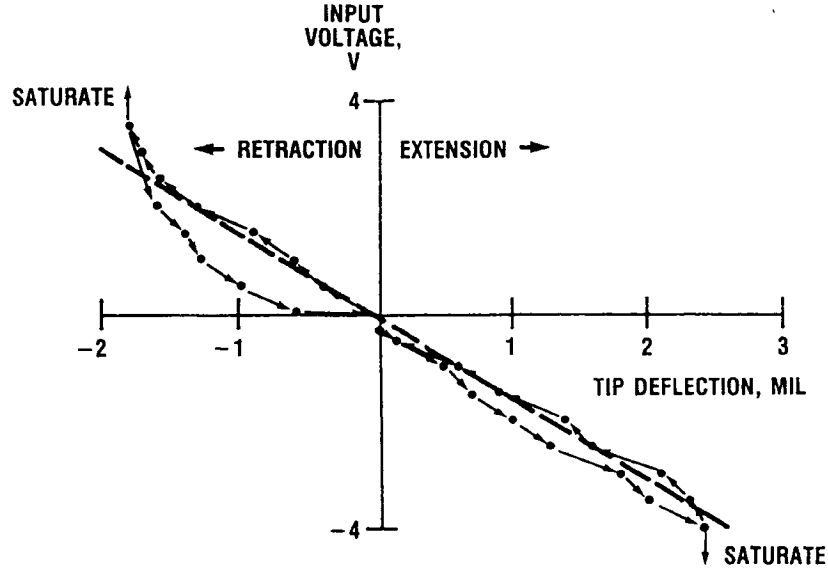

CD-88-32860

DEFLECTION VERSUS LOAD

Load deflection characteristics of the pushers, were obtained by securing each one in a solid cylinder, applying the load W, which produces reaction R on the protruding tip of the pusher, and then measuring the tip deflection. Repeated tests with three separate pushers yielded an average stiffness of approximately 20 000 lb/in.

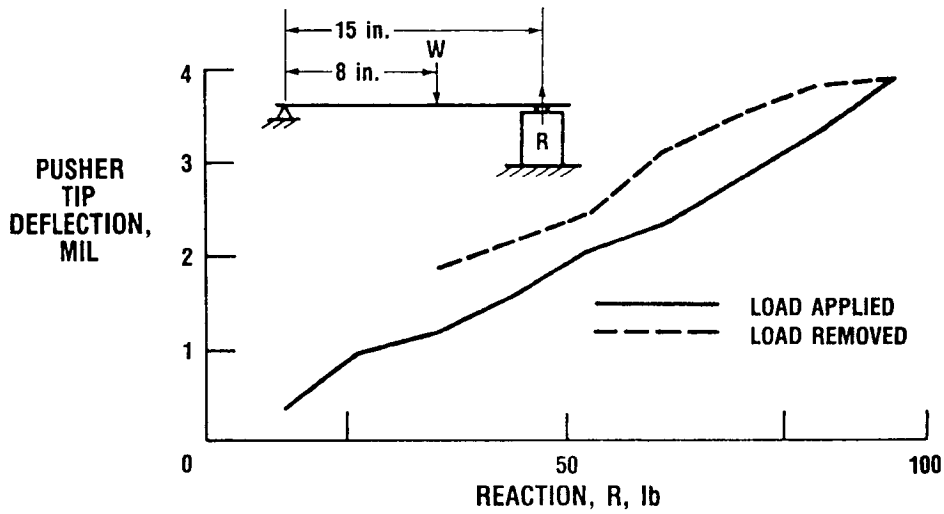

CD-88-32861

TEST RIG

This figure shows a simple sketch of the test rig, which consists of a 1-in.-diameter shaft, a 24-in.-long, 5.1-in. diameter, 3.15-lb overhung disk, and two squirrel-cage-mounted ball bearings. The outboard bearing is externally forced by an orthogonal pair of piezoelectric pushers, which are, in turn, positioned opposite the two eddy-current displacement probes d_3 and d_4. The uncoupled, velocity feedback control law used is

$$\alpha_{hor} = -G'_{hor}\,\dot{d}_4$$

$$\alpha_{ver} = -G'_{ver}\,\dot{d}_3$$

where G' represents a gain factor.

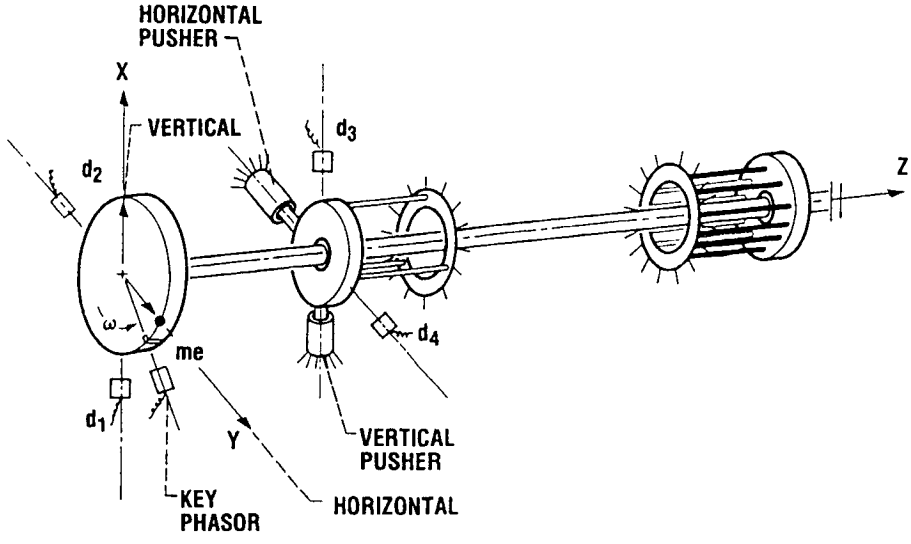

CD-88-32862

FEEDBACK CIRCUIT

This figure outlines how effective damping can be calculated once the probe and actuator sensitivities and actuator stiffness are known. The horizontal and vertical active damping were set equal in this arrangement, that is, C_A = 1.57G lb sec/in., where G is the amplifier gain.

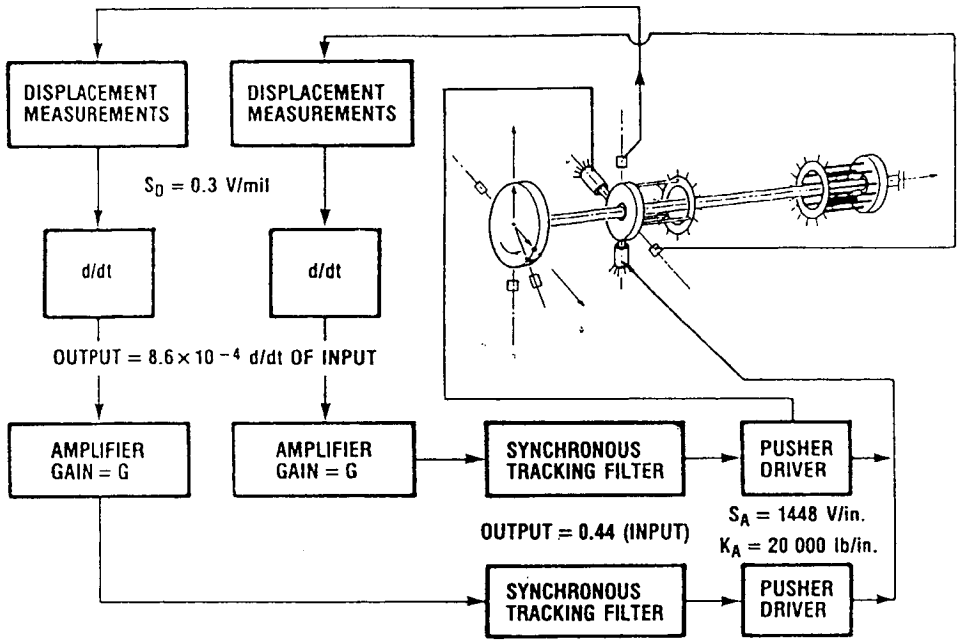

CD-88-32863

UNCOUPLED VELOCITY FEEDBACK $\alpha = G'\dot{d}$

ACTIVE DAMPING $C_A = K_A G'$

ACTUATOR INPUT VOLTAGE FOR α DISPLACEMENT, V_A

$$V_A = S_A \alpha$$

SUBSTITUTING THE DATA $V_A = S_A G' \dot{d} = 0.44\ S_D(8.6 \times 10^{-4}\dot{d})G$

RESULTS IN

$$S_A \frac{C_A}{K_A}\dot{d} = S_D \times G(3.8 \times 10^{-4})\dot{d}$$

OR

$$C_A = 3.8 \times 10^{-4} \frac{S_D}{S_A} \times G \times K_A = 1.57 \times G \text{ lb sec/in.}$$

CD-88-32864

TEST VIBRATION AMPLITUDES FOR PROBES d_1 AND d_2

The rotor was carefully balanced and then intentionally unbalanced by a known amount (0.14 oz in.), in order to compare the test results with those predicted by an unbalance response computer program. The top figure shows the test vibration amplitudes versus speed plots for the disk probe d_1. The family of curves is generated by switching amplifier gains in the feedback circuit and calculating effective damping according to the feedback relationships. The bottom figure shows the test vibration amplitudes for disk probe d_2.

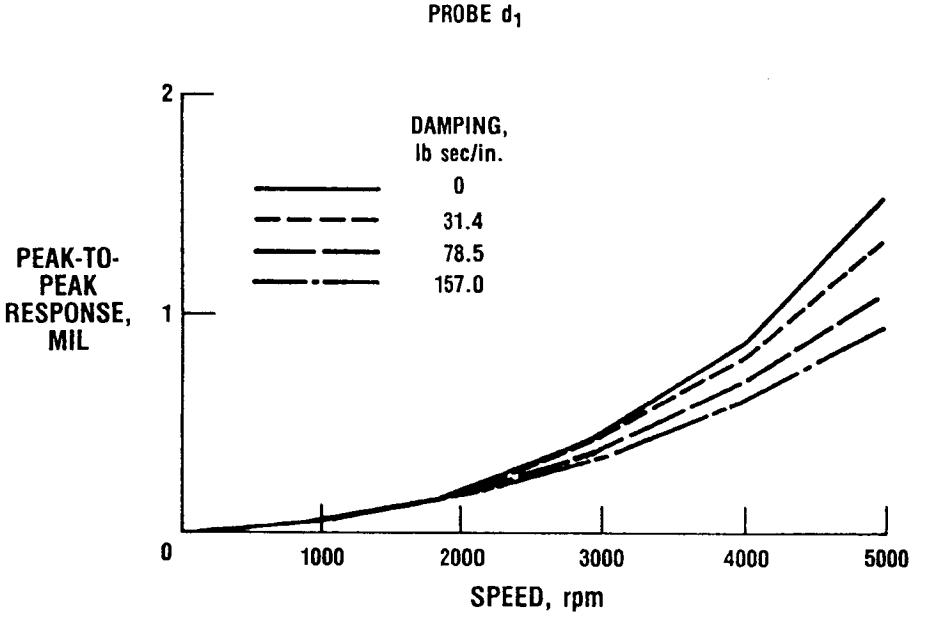

CD-88-32865

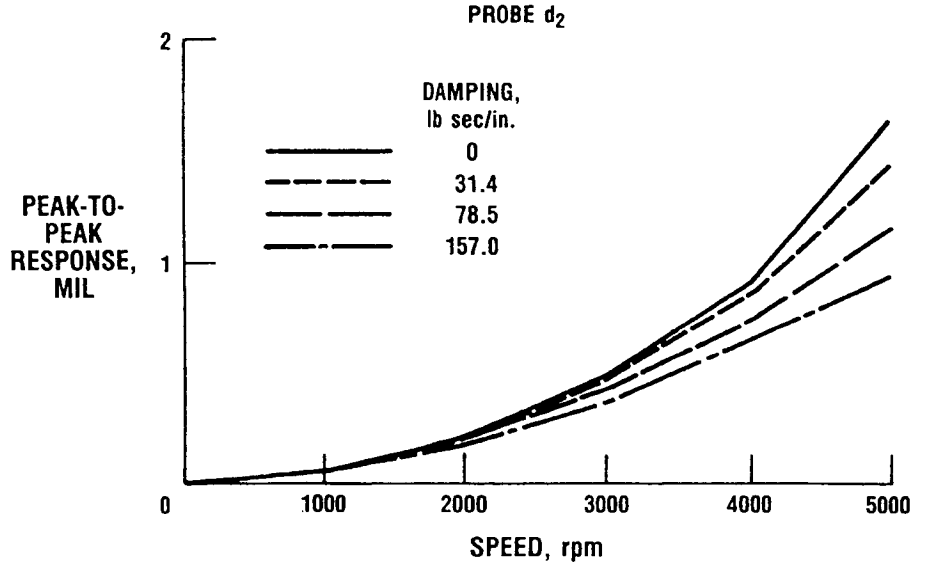

CD-88-32866

COMPUTED VIBRATION AMPLITUDES FOR PROBE d_1 OR d_2

This figure shows the computer simulation results for either probe d_1 or d_2. Although the test results show less damping than the predicted results exhibit, the trends are very similar, and the test damping is still approximately (57 lb sec/in.).

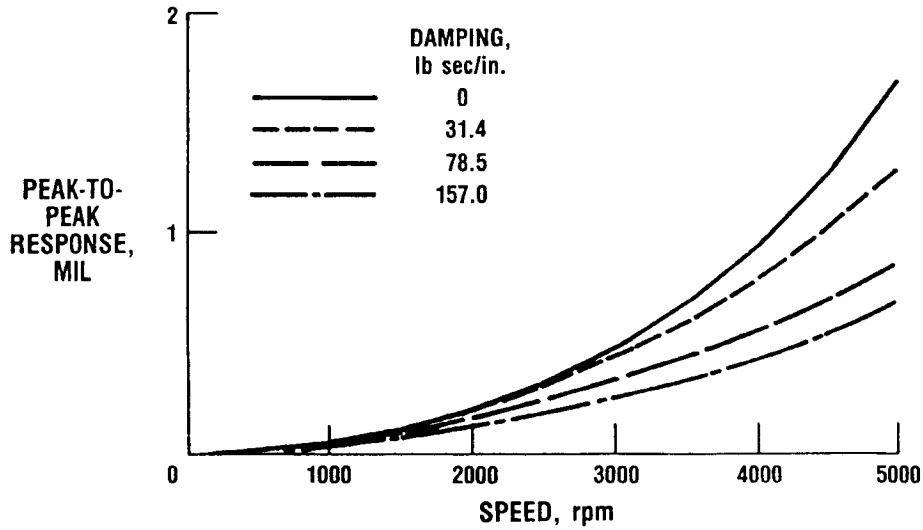

CD-88-32867

TEST VIBRATION AMPLITUDES FOR PROBES d_3 AND d_4

The top figure shows the test vibration amplitudes for the bearing housing probe d_3. The bottom figure shows the test vibration amplitudes for the bearing housing probe d_4.

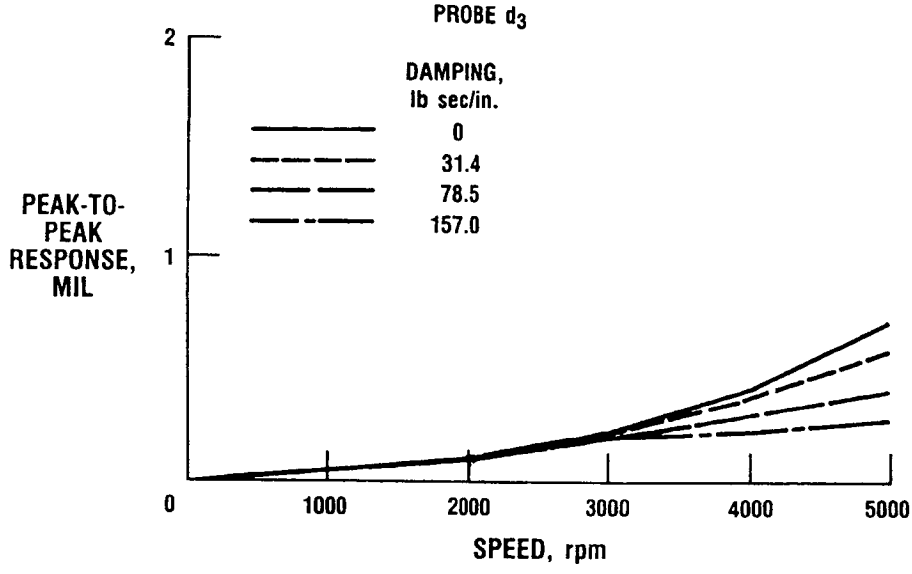

CD-88-32868

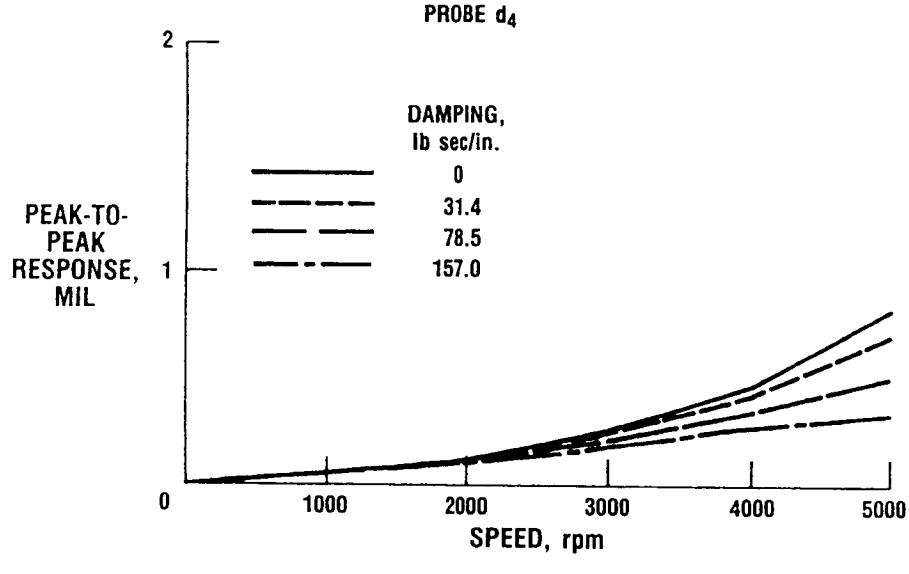

CD-88-32869

COMPUTED VIBRATION AMPLITUDES FOR PROBE d_3 OR d_4

This figure shows the computer simulation results for either probe d_3 or d_4. The results again indicate that the equation in the feedback circuit over-predicts the active damping. However, the pushers do provide approximately (80.0 lb sec/in.) damping at the highest amplifier gain setting.

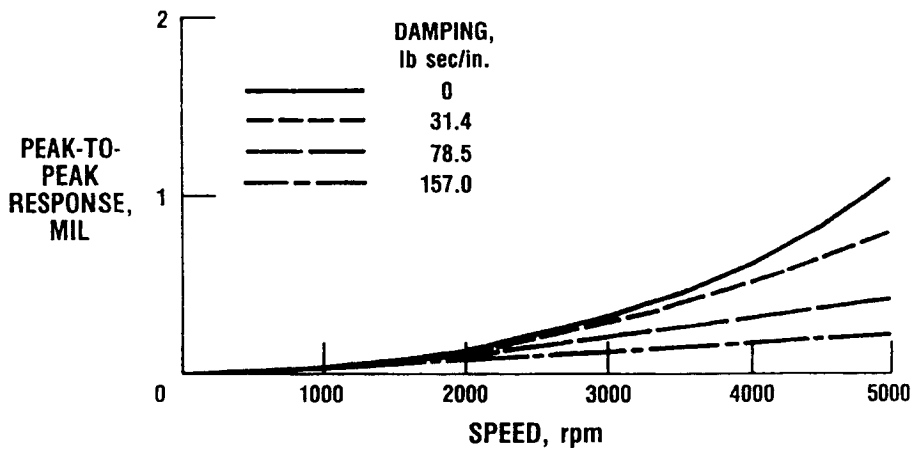

CD-88-32870

AIRCRAFT TURBINE ENGINE (T-64)

Computer simulations were performed to estimate the pusher stroke and force requirements for providing useful levels of damping in actual turbomachinery. The engine in this figure consists of a power turbine drive shaft supported by two rolling-element bearings which rotate concentrically inside a hollow gas-generator drive up to 17 000 rpm. There are four rolling-element bearings associated with the gas-generator turbine that runs between 10 500 to 18 230 rpm. The power turbine drive shaft has a span of 55.5 in. and weighs 91.5 lb. The gas-generator driveshaft is 44.2 in. long and weighs 112 lb.

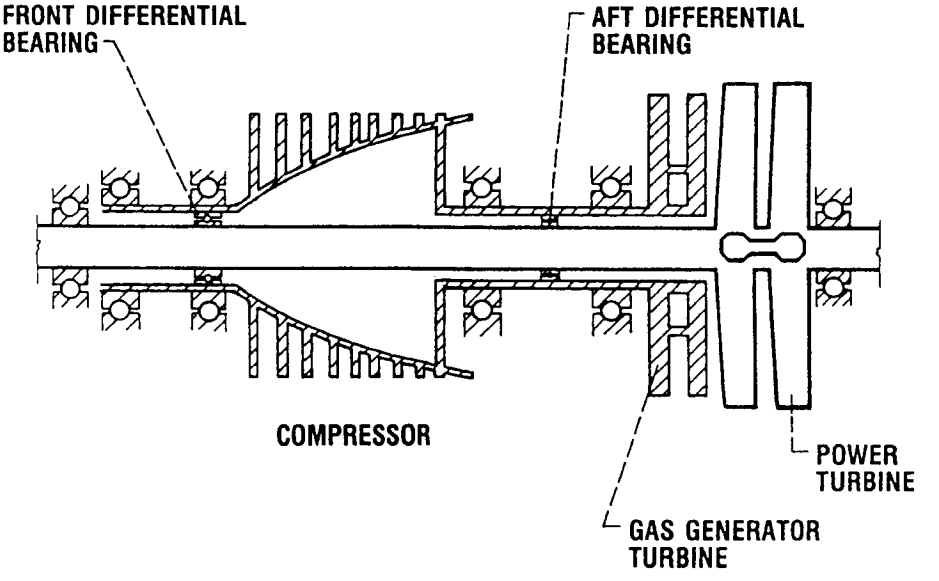

CD-88-32871

FINITE-ELEMENT MODEL

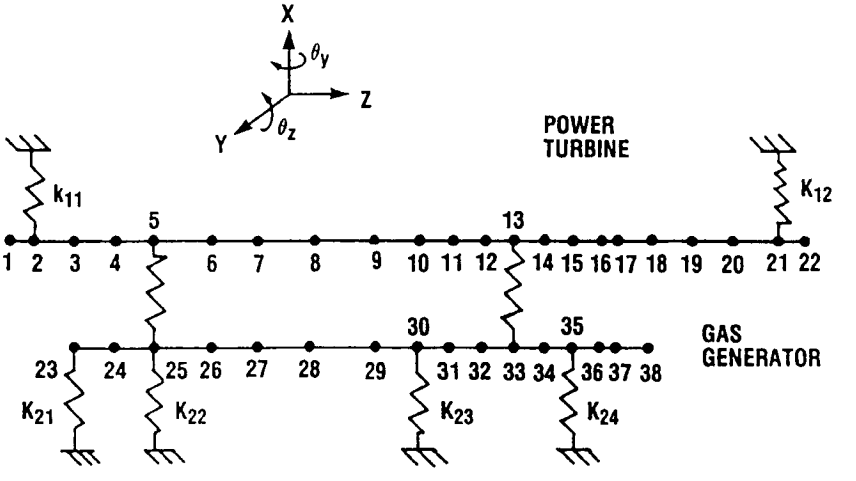

CD-88-32872

MODE SHAPE PLOTS

The plots below show the lowest, undamped forward mode, the lowest, undamped backward whirl mode, and the second, forward whirl mode for the finite-element model of each set. The upper plot is the power turbine, and the lower is the gas generator. The gas generator participation in the first, forward whirl mode is very small, but it predominates in the first, backward whirl mode. The plot for second, forward whirl mode shows participation of both power turbine and gas generator motion.

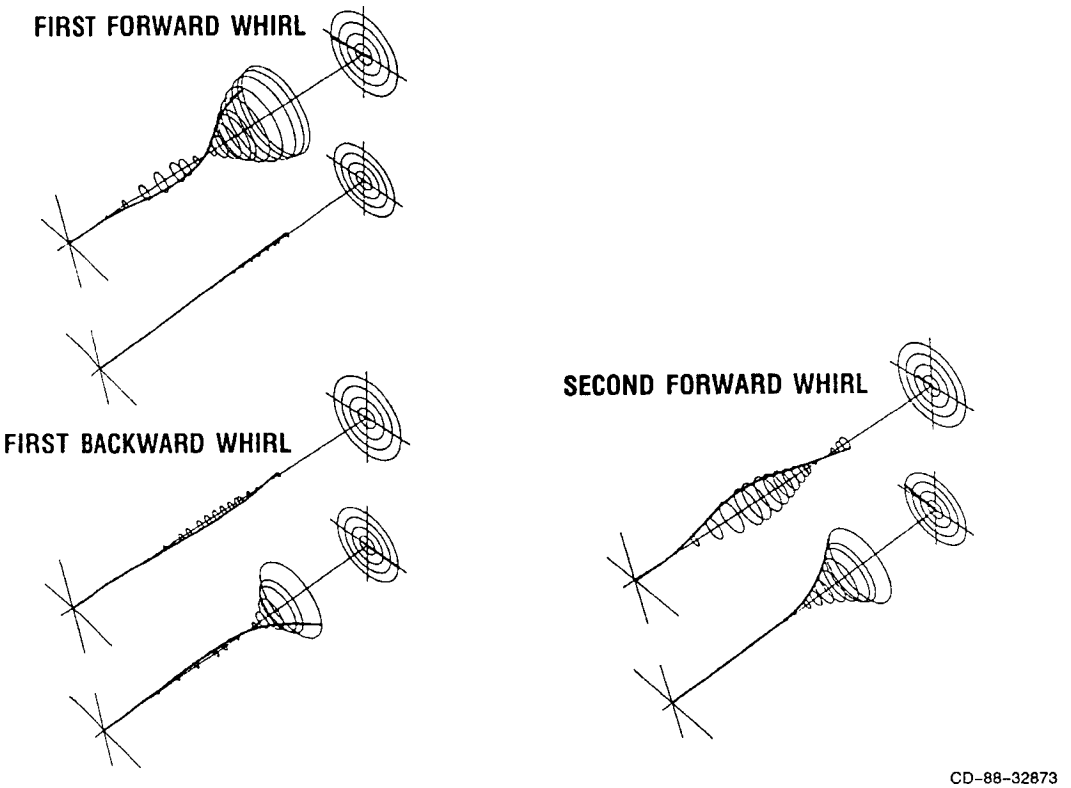

POWER TURBINE STEADY RESPONSE

This figure shows an unbalance response plot at the outboard end of the gas generator (node 36). The system is excited by out-of-phase unbalances of 0.25 oz in. at nodes 8 and 20. The damper is located at the right bearing of the power turbine (node 21). The results show that a 100 lb sec/in. damping value can significantly attenuate vibration at all critical speeds.

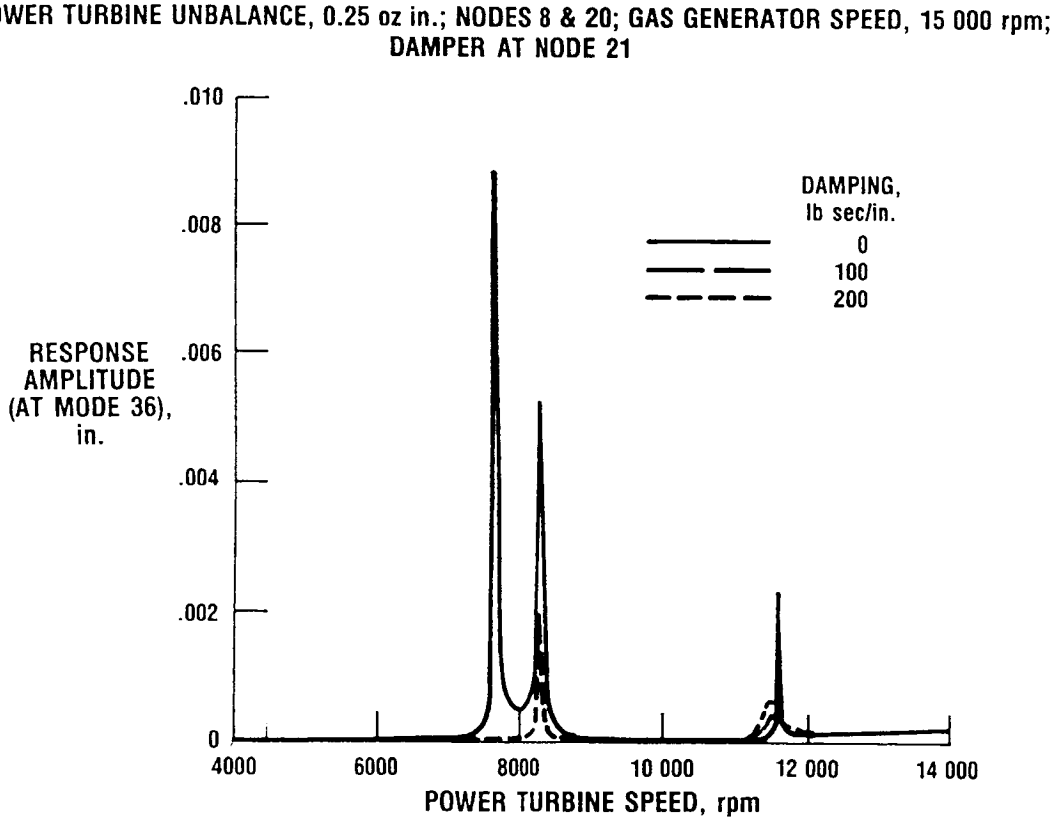

PRESCRIBED PUSHER DISPLACEMENT

This figure shows the internal displacement α of the pusher damper for the previous unbalance response run. These results are based on $\alpha = -C\dot{Z}/K$, where C is the active damping value, $\dot{Z}$ is the velocity of the pusher attachment point (node 21), and K, the assumed pusher stiffness, is 25 000 lb/in. Note that the maximum internal displacement of the pusher with C = 100 is about 4 mils.

POWER TURBINE UNBALANCE, 0.25 oz in.; NODES 8 & 20; GAS GENERATOR SPEED, 15 000 rpm; DAMPER AT NODE 21; PUSHER STIFFNESS, 25 000 lb/in.

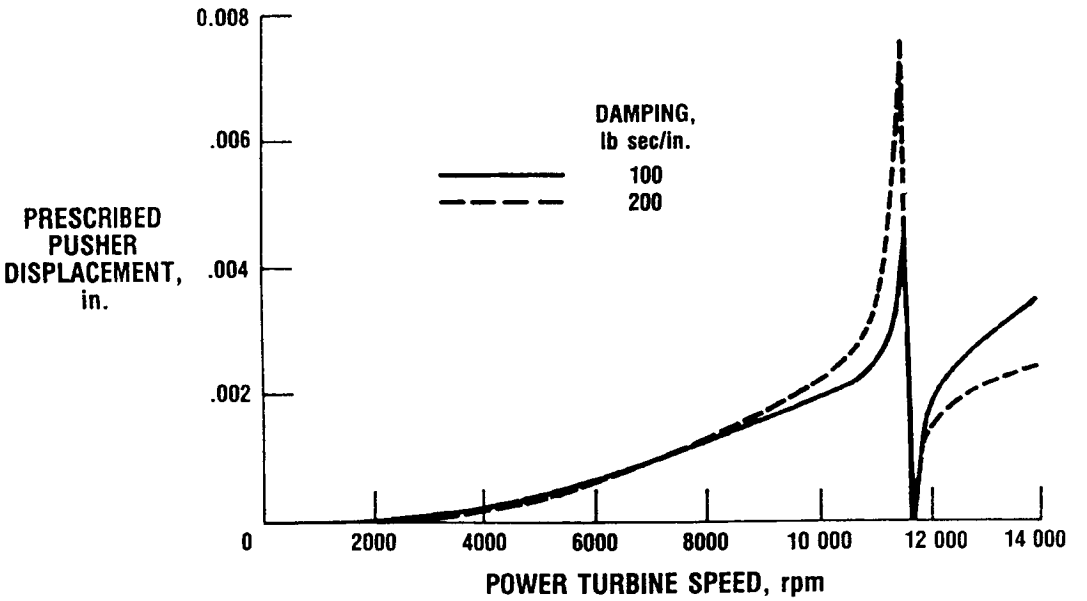

CD-88-32875

REQUIRED PUSHER FORCE VERSUS SPEED

The plot shows pusher force (pusher stiffness times (Z - α) versus speed) for the previous unbalance response run. The maximum pusher force with C = 100 is approximately 100 lb.

POWER TURBINE UNBALANCE, 0.25 oz in.; NODES 8 & 20; GAS GENERATOR SPEED, 15 000 rpm;
DAMPER AT NODE 21; PUSHER STIFFNESS, 25 000 lb/in.

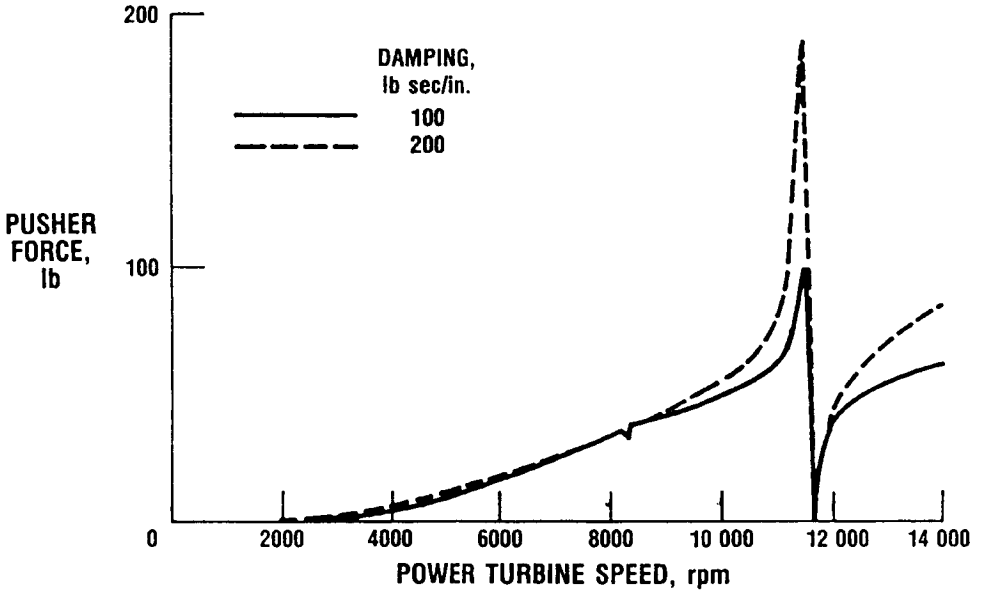

CD-88-32876

POWER TURBINE STEADY RESPONSE

This figure shows the same response as in the previous case. However, the damper is now located at the outboard bearing of the gas generator, that is, at node 36. At this location the damper is ineffective in controlling the lowest mode. This results because the gas generator does not participate in this mode, as shown in the mode shape plots.

POWER TURBINE UNBALANCE, 0.25 oz in.; NODES 8 & 20; GAS GENERATOR SPEED, 15 000 rpm; DAMPER AT NODE 36; PUSHER STIFFNESS, 25 000 lb/in.

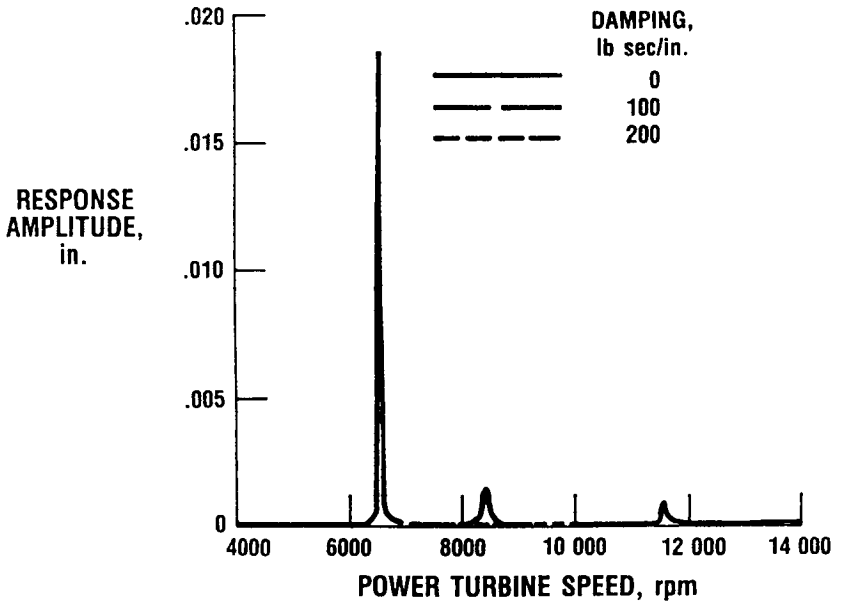

CD-88-32877

VARIATION OF REAL PART VERSUS CROSS-COUPLED STIFFNESS

This rotor-bearing system is unstable if the damper is removed and an Alford type cross couple stiffness of 1000 lb/in. is applied at node 37. The unstable eigenvalue is 3.3 sec^{-1} at 12 390 rpm. This figure shows the real part of the same eigenvalue when a 100-lb sec/in.-damper is installed at node 35. The previously unstable mode is seen to be stable even with a cross-coupled stiffness of 10 000 lb/in.

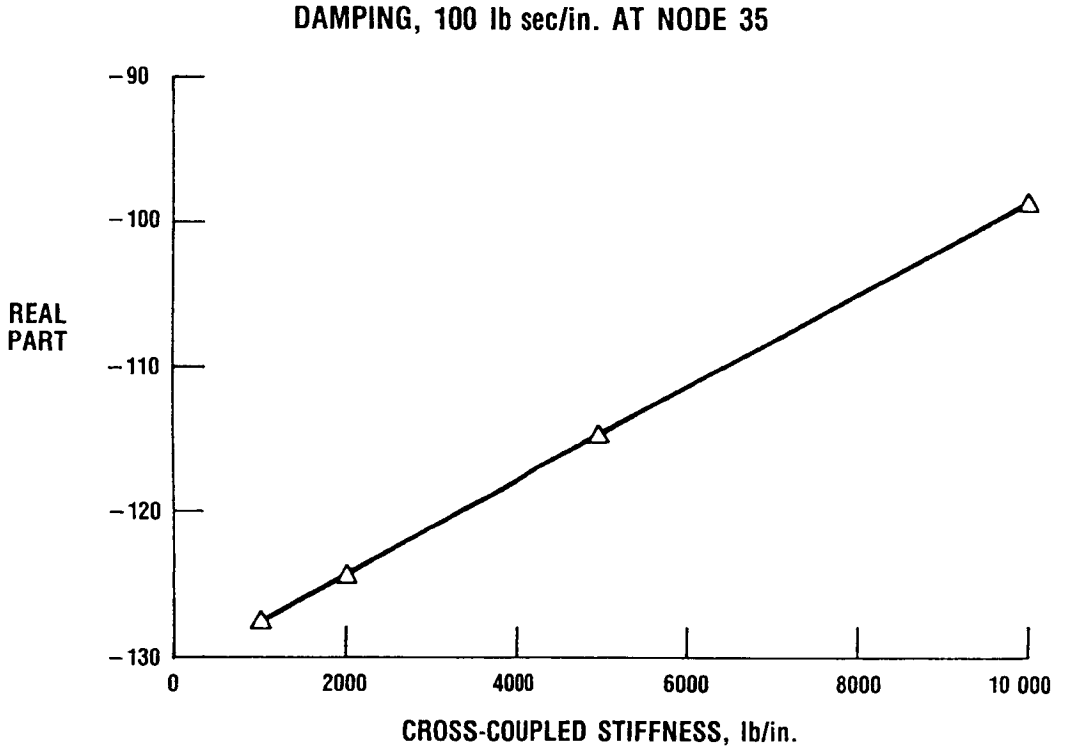

CD-88-32878

SUMMARY

This presentation has examined the potential use of piezoelectric pushers for active control of rotor-bearing system vibrations. The results showed significant levels of active damping contributed by the pushers (50 to 80 lb sec/in.) and very good agreement between vibration response trends predicted by theory and measured on the rig. Finite-element computer simulations showed that significant improvements in rotor stability and unbalance response could be achieved with an active damping of 100 lb sec/in., which requires a pusher with displacement of about 4 mils, force of 100 lb, and a stiffness of 25 000 lb/in.

- PIEZOELECTRIC PUSHERS APPLIED TO ACTIVE CONTROL OF ROTOR-BEARING SYSTEM VIBRATIONS
- TESTING CONDUCTED AT NASA LEWIS SHOWED SIGNIFICANT LEVELS OF ACTIVE DAMPING
- COMPUTER SIMULATIONS SHOWED PIEZOELECTRIC PUSHERS EFFECTIVELY CONTROLLED VIBRATION IN ENGINES.

CD-88-32879